# Whirl Flutter Stability Analysis of a Tiltrotor Aircraft Including Various Aerodynamic Models

**Taeseong Kim[1] and SangJoon Shin[2]**

[1] School of Mechanical and Aerospace Engineering
Building 301 Room 1313, Seoul National University, 56-1, Shillim-dong, Kwanak-gu, Seoul, Korea
e-mail: kimts77@snu.ac.kr

[2] School of Mechanical and Aerospace Engineering
Building 301 Room 1418, Seoul National University, 56-1, Shillim-dong, Kwanak-gu, Seoul, Korea
e-mail: ssjoon@snu.ac.kr

**Key words:** whirl flutter, unsteady aerodynamics, tiltrotor aircraft

**Abstract:** The whirl flutter instability imposes a serious limit on the maximum forward flight speed of tiltrotor aircraft, and therefore many researches are conducted to improve this instability. In this paper, an analysis is formulated to predict an aeroelastic stability of a gimballed three-bladed rotor with a flexible control system and flexible wing based on three different types of aerodynamic models, which are normal quasi-steady, Greenberg quasi-steady and unsteady aerodynamic forces. Numerical results are obtained in both time and frequency domains. Generalized eigenvalue and Runge-Kutta methods are utilized to estimate whirl flutter stability in frequency and time domain, respectively.

## INTRODUCTION

Tiltrotor is one of the advanced aircrafts currently under significant development, and it has a higher cruise speed and larger payload capability than the conventional helicopter does. This aircraft does not require a long runway for taxing, take-off, and landing. There are two modes, which are the helicopter and airplane mode. For takeoff and landing, tiltrotor aircraft tilts the rotor system vertically, which is attached at the end of wing. This is called as a helicopter mode at which vertical takeoff and landing is possible like a conventional helicopter. For a cruise flight, the rotor system is tilted forward like a turboprop aircraft. It is an airplane mode at which tiltrotor aircraft may have a high cruise speed. However, during the high cruise flight condition, the whirl flutter phenomenon appears.

The whirl flutter instability, which is induced by the inplane hub forces, generally imposes a limit on the cruise performance in tiltrotor aircrafts. It involves two modes of the tiltrotor aircrafts, which are a rotor and a pylon mode. The rotor mode is the backward whirl mode which occurs at low frequencies, while the pylon mode is the forward whirl mode whose flutter frequencies are near the natural frequencies of the aircraft system. Flutter frequencies of the pylon mode are higher than those associated with flutter in the rotor mode. There exists a significant difference between the two flutter mechanisms. In the pylon mode the precession is in the same direction as the rotor blade rotation. On the other hand, the precession of the rotor mode is in the opposite direction. It has been found that the whirl flutter instability occurs more frequently in the rotor mode because of the low frequencies [1, 2].

Precise estimation of the whirl flutter instability is required to enhance the cruise performance. Many researches have been conducted to increase aeroelastic stability boundary using several design parameters. Hall [1] analyzed the principal destabilizing factors for rotor/pylon whirl

flutter. They are the rotor pylon mounting stiffness and pitch-flap coupling. Based on his research, the stability boundary is decreased when the rotor pylon mounting stiffness is reduced and the pitch-flap coupling is increased. The fundamental flap frequencies to enhance the aeroelastic stability boundary are examined by Young and Lytwyn [3]. The precise flapping frequency is determined between 1.1 and 1.2/rev by static and dynamic stability trend. Johnson [4] performed a rigid-blade analysis and validated it with the experimental data. He extended the analysis to utilize the coupled blade bending and torsion modes, and the non-axial flow, which enabled the analysis of the helicopter mode and the conversion operation [5, 6]. He examined that the blade torsion dynamics was the most affecting parameter to introduce the whirl flutter instability.

To improve the aeroelastic stability boundary, active control methodologies are conducted. Harmonic Control (HHC) was experimentally employed at both the rotor swashplate and the wing flaperon to reduce vibrations in airplane mode [7]. In Ref. 8, Generalized Predictive Control (GPC) was experimentally investigated to evaluate the effectiveness of an adaptive control algorithm. More recently, refined active control algorithm employed via actuation of the wing flaperon and the rotor swashplate was examined for whirl flutter stability and robustness augmentation [9].

However, it is observed that the previous analytical investigations have not considered an unsteady aerodynamic effect, which is necessary to examine the phenomenon in a real operating environment. In this paper, a comprehensive analysis is developed to accurately predict and enhance the whirl flutter instability both in time and frequency domain with a 9 degree-of-freedom model. The considered model includes the flapping and lead-lag motion of the rotor with a flexible control system and flexible wing motion.

## 1. ANALYCAL MODELING

### 1.1 Structural modeling

The structural model of the tiltrotor aircraft, which is presented in Fig. 1, is developed based on Ref. 4. It is very similar to a typical helicopter structural configuration; however, a few modifications are needed because of several additional degrees of freedom such as the rotor precone, shaft, and the wing. The present model basically consists of nine degrees of freedom, which are three rotor blade flapping ( $\beta_0$, $\beta_{1C}$ and $\beta_{1S}$ ), lead-lag ( $\zeta_0$, $\zeta_{1C}$ and $\zeta_{1S}$ ) motions of the the rotor, and three elastic wing ( $q_1$, $q_2$ and $p$ ) motions for quasi-steady aerodynamic environment. In case of the full unsteady aerodynamic model, four more degrees of freedom are required, which are augmented state variables ( $X_{1C}$, $X_{1S}$, $X_{2C}$, and $X_{2S}$ ) for aerodynamics. They are explained in detail in the Refs. 10 and 11.

Using the force and moment equilibrium, the rotor, shaft, and wing equations of motion are obtained. Among them the rotor and shaft equations of motion are obtained in a rotating frame. Therefore, Fourier coordinate transformation is employed in order to convert these equations into those in a non-rotating frame.

In this paper, one of the most important factors of the modeling is the blade flexibility with a pitch-flap ( $K_{p\beta}$ ) and pitch-lag ( $K_{p\zeta}$ ) coupling. The effective coupling parameters with respect to the aircraft flight speed, which is presented in Fig. 2, are adapted from Refs. 4 and 12.

The final form of the structural equation is arranged in the left hand side (LHS) in governing equations, while the aerodynamic equation is in the right hand side (RHS) of the same equation. The more detail expressions of equation are presented in Ref. 11.

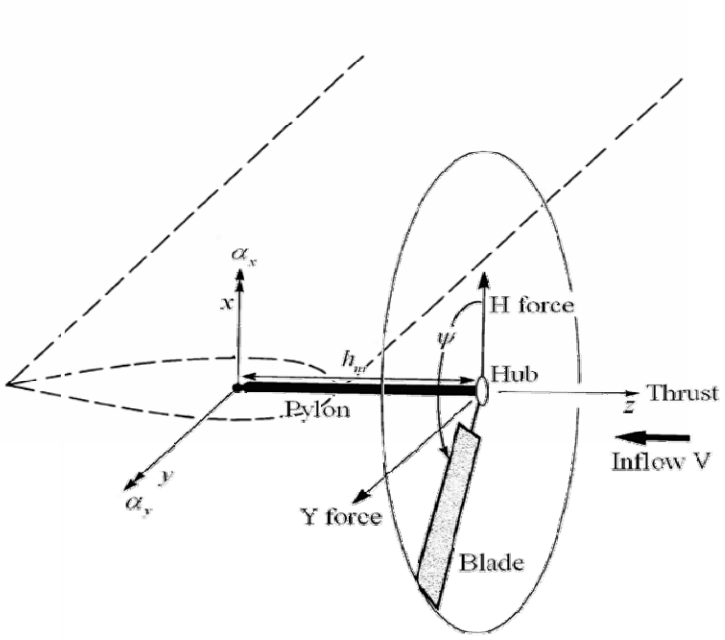


*Figure 1. A rotor system with a completely rigid blade*

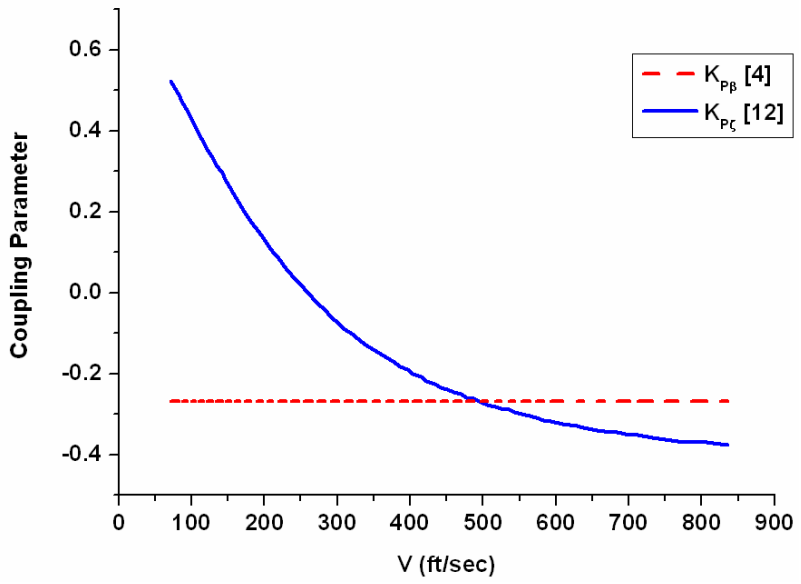


*Figure 2. Effective pitch-flap and pitch-lag coupling parameter variation*

## 1.2 Aerodynamic modeling

The aerodynamic formulations are obtained with an assumption that the tiltrotor aircraft is in a purely axial flow in equilibrium. Only a perturbation component in aerodynamics is considered in this paper. Trim state is assumed to be established already and the perturbation from it is considered for flutter analysis. The perturbation velocities are defined as follows.

$$\delta U = \frac{u_{T_0}}{U_0}\delta u_T + \frac{u_{p_0}}{U_0}\delta u_p \tag{1}$$

$$\delta u_p = r(\dot{\beta} - \dot{\alpha}_y \cos\psi_m + \dot{\alpha}_x \sin\psi_m) + (Vu_G + \dot{z}_P) = r\delta u_{p_B} + \delta u_{p_A} \tag{2}$$

$$\begin{aligned}\delta u_T &= r(\dot{\alpha}_Z - \dot{\varsigma}) - h_m(\dot{\alpha}_y \sin\psi_m + \dot{\alpha}_x \cos\psi_m) + (V+v)(\alpha_y \sin\psi_m + \alpha_x \cos\psi_m) \\ &\quad + V(\beta_G \cos\psi_m + \alpha_G \sin\psi_m) + (\dot{y}_P \cos\psi_m - \dot{x}_P \sin\psi_m) \\ &= r\delta u_{T_A} + \delta u_{T_B}\end{aligned} \tag{3}$$

$$\delta\theta = \bar{\theta} - K_{p\beta}\beta - K_{p\varsigma}\varsigma \tag{4}$$

where $\bar{\theta}$ is control input.

In this paper, three different kinds of aerodynamic model are developed to predict whirl flutter stability both in time and frequency domains. Those are two quasi-steady and an unsteady aerodynamic model. The first aerodynamic model is widely used and is quoted as a normal quasi-steady aerodynamics in this paper. This aerodynamic model is developed based on Ref. 4. The second quasi-steady aerodynamic model is cited as Greenberg's quasi-steady aerodynamic model in this paper whose detailed equation is described in Eq. (6). It is equivalent to replacing $C(k)$ by 1 in Greenberg's aerodynamic model [13, 14]. For a full unsteady aerodynamic representation, Greenberg's two-dimensional unsteady aerodynamic model is used [14]. Its expression is also presented in Eq. (7). Both in Greenberg's quasi-steady and in full unsteady aerodynamic model, noncirculatory terms are ignored. Since a thin airfoil theory is adapted in the present derivation, the effects of noncirculatory terms are very small compared with the circulatory ones [15].

$$L = 2\pi\rho U(t)^2 b\alpha(t) \tag{5}$$

$$L = \underbrace{2\pi\rho U(t)b[(\dot{h}(t) + U(t)\theta(t)) + b(\frac{1}{2} - a_h)\dot{\theta}(t)_{ref}]}_{Circulatory\ part(L_C)} + \underbrace{\pi\rho b^2[(\dot{h}(t) + U(t)\theta(t))\dot{} - ba_h\ddot{\theta}(t)_{ref}]}_{Noncirculatory\ part(L_{NC})} \tag{6}$$

$$\begin{aligned}L = &\underbrace{2\pi\rho U(t)bC(k)[(\dot{h}(t) + U(t)\theta(t)) + b(\frac{1}{2} - a_h)\dot{\theta}(t)_{ref}]}_{Circulatory\ part(L_C)} \\ &+ \underbrace{\pi\rho b^2[(\dot{h}(t) + U(t)\theta(t))\dot{} - ba_h\ddot{\theta}(t)_{ref}]}_{Noncirculatory\ part(L_{NC})}\end{aligned} \tag{7}$$

where $\dot{h}(t) = -\delta u_p(t)cos\phi + \delta u_T(t)sin\phi$.

The aerodynamic environment of the typical rotor blade section is presented in Fig. 3. All the velocities and forces are estimated with respect to the hub plane. The aerodynamic forces acting on a blade typical section are lift (L) and drag (D). Therefore using a life and drag forces, the total forces in x and z direction can be obtained [11]. However the aerodynamic forces acting on a blade are dominated by the lift in a rotor flow field with a high inflow. Thus, the drag forces are not included and only the $C_{l\alpha}$ terms are retained.

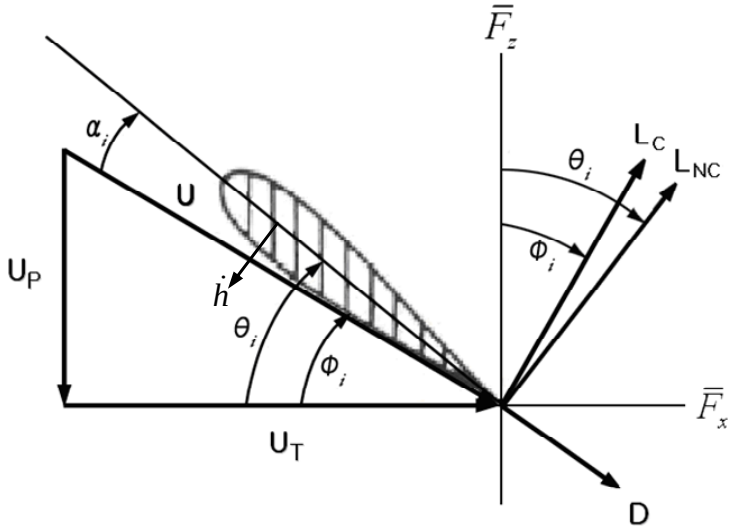


*Figure 3 : Resultant and inflow velocity on a typical blade section*

For the full unsteady aerodynamic model, the equations of forces and moments are slightly different because of the lift deficiency function, $C(k)$, which is represented only in frequency domain. Therefore Jones' approximation is utilized to predict the stability boundary in time domain [16, 17]. The new state-space equations for the augmented state variables and circulatory part of the lift can be formulated as a dimensionless form because of the modified lift deficiency function. The augmented state variables are associated with a downwash velocity at the three quarter chord location [18]. They describe the unsteady effects. In this paper the augmented state variables of the typical section at $3/4$ span location are utilized as an averaged value.

## 2. FLUTTER STABILITY ANALYSIS

After the rotor aerodynamic forces and moments are formulated with the $C_{l\alpha}$ term, they need to be assembled in the structural equations. Therefore they are substituted into the RHS in the governing equations. Then, the final forms are obtained with the nine and thirteen degrees of freedom for the quasi-steady and full unsteady aerodynamics, respectively. First of all, the governing equations with quasi-steady aerodynamic models are given below. The governing equations for the normal and Greenberg's quasi-steady aerodynamic models result in the same form.

### 2.1 Quasi-steady aerodynamic models

Putting the forces and moments of the rotor into the RHS of the governing equation gives the following expression.

$$RHS = C_a\dot{y} + K_a y + G_a p + Z_a g \tag{8}$$

where $y^T = \{\beta_{1C} \quad \beta_{1S} \quad \varsigma_{1C} \quad \varsigma_{1S} \quad \beta_0 \quad \varsigma_0 \quad q_1 \quad q_2 \quad p\}$, $p^T = \{\theta_{1C} \quad \theta_{1S} \quad \theta_0\}$,
$g^T = \{u_G \quad \beta_G \quad \alpha_G\}$, and the subscript *a* means an aerodynamic part.

The final form of the governing equation can be rewritten as follows.

$$M_s\ddot{y} + C_s\dot{y} + K_s y = C_a\dot{y} + K_a y + G_a p + Z_a g \tag{9}$$

where the subscript *s* means a structural part and all elements of the matrices are dimensionless.

For simplicity, Eq. (9) can be rearranged as

$$\begin{aligned} M_s\ddot{y} &= -(C_s - C_a)\dot{y} - (K_s - K_a)y + G_a p + Z_a g \\ \therefore \ddot{y} &= -M_s^{-1}(C_s - C_a)\dot{y} - M_s^{-1}(K_s - K_a)y + M_s^{-1}G_a p + M_s^{-1}Z_a g \\ &= -(M_s^{-1}\bar{C})\dot{y} - (M_s^{-1}\bar{K})y + M_s^{-1}G_a p + M_s^{-1}Z_a g \\ &= -A\dot{y} - By + \bar{G}p + \bar{Z}g \end{aligned} \tag{10}$$

where, $\bar{C} = (C_s - C_a)$, $\bar{K} = (K_s - K_a)$, $A = (M_s^{-1}\bar{C})$, $B = (M_s^{-1}\bar{K})$, $\bar{G} = (M_s^{-1}G_a)$ and
$\bar{Z} = (M_s^{-1}Z_a)$.

Converting Eq. (10) into a state space form gives

$$\dot{Y} = \underbrace{\begin{bmatrix} 0 & I \\ -B & -A \end{bmatrix}}_{18\times18}\underbrace{\begin{Bmatrix} y \\ \dot{y} \end{Bmatrix}}_{18\times1} + \underbrace{\begin{bmatrix} 0 & 0 \\ \bar{G} & \bar{Z} \end{bmatrix}}_{18\times6}\underbrace{\begin{Bmatrix} p \\ g \end{Bmatrix}}_{6\times1} \tag{11}$$

where $Y^T \equiv \{y \quad \dot{y}\}$.

### 2.2 Full unsteady aerodynamic model

Adopting Jones' approximation, the state space equations for the augmented state variables and circulatory part of the lift can be formulated as a dimensionless form below.

$$\begin{Bmatrix} \dot{\bar{X}}_1 \\ \dot{\bar{X}}_2 \end{Bmatrix} = \begin{bmatrix} a_{11} & a_{12} \\ 1 & 0 \end{bmatrix}\begin{Bmatrix} \bar{X}_1 \\ \bar{X}_2 \end{Bmatrix} + \begin{Bmatrix} 1 \\ 0 \end{Bmatrix}Q(\psi) \tag{12}$$

$$\bar{L}_c = 2\pi b U(\psi)\left\{C\bar{X}_1 + D\bar{X}_2 + 0.5Q(\psi)\right\} \tag{13}$$

where where, $Q(\psi) = \left[(\dot{h}(\psi) + U(\psi)\theta(\psi)) + b(\frac{1}{2} - a_h)\dot{\theta}(\psi)_{ref}\right]$.

Substituting the aerodynamic forces and moments with new calculated circulatory part of the lift, which is presented in Eq. (13), into the structural equations, a state space equation is obtained as follows.

$$\dot{Y} = \underbrace{\begin{bmatrix} 0 & I \\ -B & -A \end{bmatrix}}_{18\times18} \underbrace{\begin{Bmatrix} y \\ \dot{y} \end{Bmatrix}}_{18\times1} + \underbrace{\begin{Bmatrix} 0 \\ C \end{Bmatrix}}_{18\times4} \underbrace{X}_{4\times1} + \underbrace{\begin{bmatrix} 0 & 0 \\ \bar{G} & \bar{Z} \end{bmatrix}}_{18\times6} \underbrace{\begin{Bmatrix} p \\ g \end{Bmatrix}}_{6\times1} \tag{14}$$

where $X^T = \left( \bar{X}_{1C} \quad \bar{X}_{1S} \quad \bar{X}_{2C} \quad \bar{X}_{2S} \right)$.

The equations of the augmented state variables describe the unsteady effects due to downwash at 1/4 chord point. Using the Eqs. (12) and (14), a governing equation, which enables analysis both in time and frequency domains, is obtained in a state-space form.

$$\begin{bmatrix} \dot{Y} \\ \dot{X} \end{bmatrix} = \underbrace{\begin{bmatrix} \underbrace{T^*}_{18\times18} & \underbrace{S^*}_{18\times4} \\ \underbrace{D}_{4\times18} & \underbrace{E}_{4\times4} \end{bmatrix}}_{22\times22} \underbrace{\begin{bmatrix} Y \\ X \end{bmatrix}}_{22\times1} + \underbrace{\begin{bmatrix} \underbrace{O^*}_{18\times6} \\ \underbrace{0}_{4\times6} \end{bmatrix}}_{22\times6} \underbrace{\begin{bmatrix} p \\ g \end{bmatrix}}_{6\times1} \tag{15}$$

where $T^* = \underbrace{\begin{bmatrix} 0 & I \\ -B & -A \end{bmatrix}}_{18\times18}$, $S^* = \underbrace{\begin{Bmatrix} 0 \\ C \end{Bmatrix}}_{18\times4}$, $\mathrm{O}^* = \underbrace{\begin{bmatrix} 0 & 0 \\ \bar{G} & \bar{Z} \end{bmatrix}}_{18\times6}$, $E = \begin{bmatrix} a_{11} & a_{12} \\ 1 & 0 \end{bmatrix}$, $D = \begin{Bmatrix} 1 \\ 0 \end{Bmatrix}$, $v = \underbrace{\begin{Bmatrix} p \\ g \end{Bmatrix}}_{6\times1}$,

$A = (\bar{M}^{-1}\bar{C})$, $B = (\bar{M}^{-1}\bar{K})$, $C = (\bar{M}^{-1}Z_a)$, $\bar{M} = (M_s - M_a)$, $\bar{C} = (C_s - C_a)$, $\bar{K} = (K_s - K_a)$, $\bar{G} = (M_s{}^{-1}G_a)$, and $\bar{Z} = (M_s{}^{-1}Z_a)$.

## 3. NUMERICAL RESULTS

Numerical investigation is conducted to obtain the aeroelastic stability boundary with the three different kinds of aerodynamic model. An autorotation condition is considered as a rotor operating condition. Autorotation means no restraint imposed on the rotor rotation about the hub. Therefore, no rotor torque is transmitted to the shaft, and no pylon roll motion is transmitted to the rotor. Since the perturbations in the control pitch input and gust are not considered in the present analysis, $\bar{G}$, $\bar{Z}$, and $O^*$ matrices may be ignored in Eqs. (11) and (15). The numerical values of the structural parameters are based on Ref. 4.

### 3.1 Comparison with other existing results

The present analysis is validated against other numerical results provided in Refs. 5, 12, and 19. The present results are in good agreement with the references. The vertical wing mode ($q_1$) comparison is illustrated in Fig. 4.

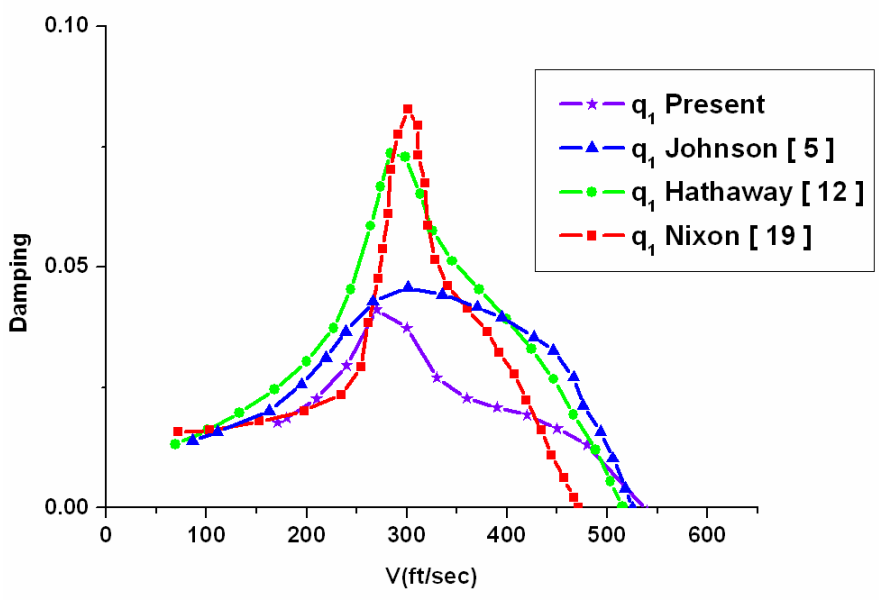


*Figure 4 : Damping of the vertical wing mode in terms of the flight speed*

### 3.2 Normal quasi-steady aerodynamic model

This section presents the results of the normal quasi-steady aerodynamic model. Figure 5 shows the predicted damping of each mode in terms of the tiltrotor flight speed. The vertical wing mode ( $q_1$ ) becomes unstable first among the modes considered. Furthermore $q_2$ and $p$ modes become consecutively unstable. Therefore only the wing degrees of freedom should be concerned.

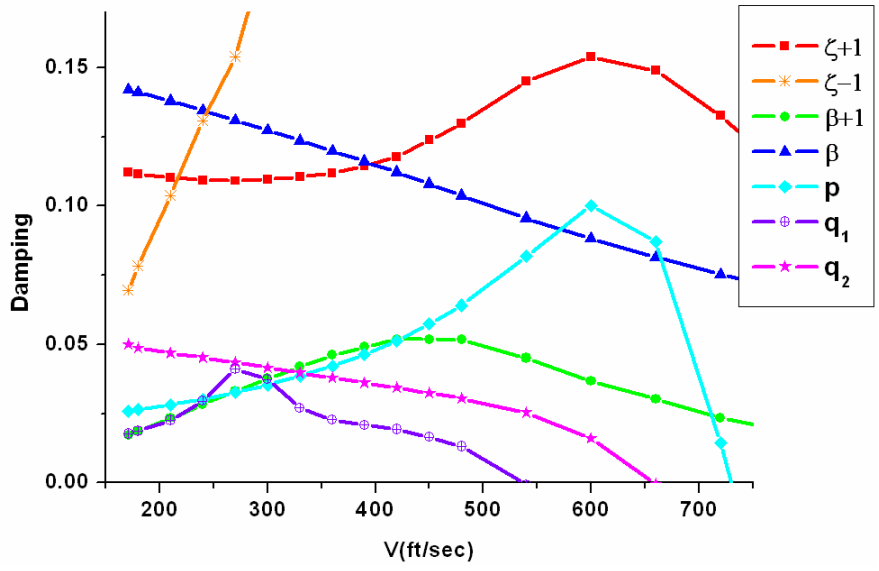


*Figure 5 : Damping of the modes in terms of the flight speed*

Figures 6 describes the results obtained in time and frequency domain respectively, while numerically increasing the flight speed from 480 to 570 ft/sec to find stability boundary. Figure 6(a) shows only the results of the wing modes in time domain. It is shown that the magnitude of each mode remains stable till V =534 ft/sec. However, it is increased when its

flight speed exceeds 534 ft/sec. Figure 6(b) shows the $q_1$ and $q_2$ mode results through the frequency domain analysis at the same flight speed. When the poles of the vertical bending mode of the wing are located on an imaginary axis, the aircraft is on the verge of flutter stability. If they are located in the right half plane, the system is unstable. Based on the present aerodynamic model, it is observed that stability boundary is approximately 534 ft/sec, which is considered to be a realistic whirl flutter boundary for the present tiltrotor aircraft.

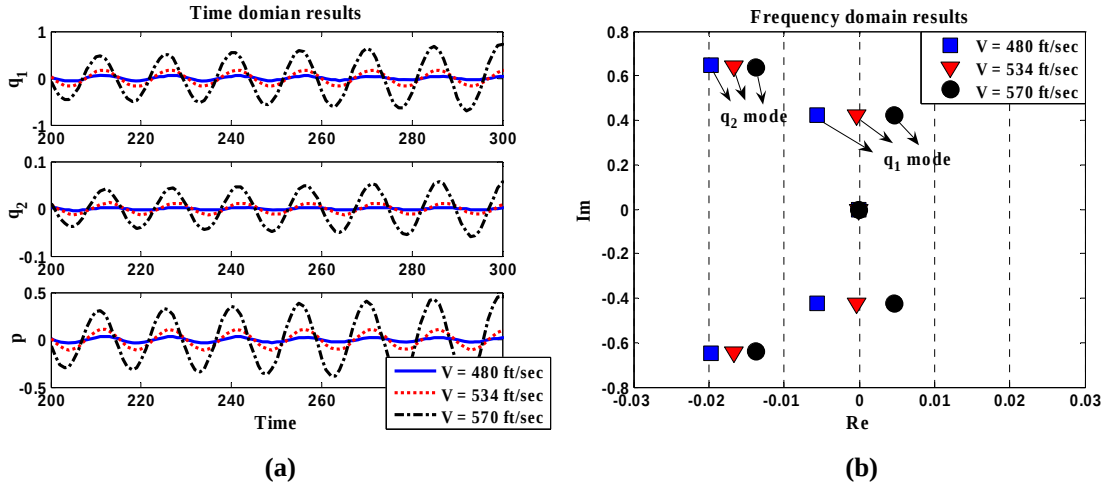


**(a)** **(b)**

*Figure 6 : Time and frequency domain analysis using the normal quasi-steady aerodynamics*

### 3.3 Greenberg's quasi-steady aerodynamic model

The second aerodynamic model has a similar formulation with that for the normal quasi-steady aerodynamics. However, the lift formulation has a few different terms. According to Eq. (6), a few first-order time derivative terms, which are $\dot{h}$ and $\dot{\theta}_{ref}$, are newly included in Greenberg's quasi-steady aerodynamic formulation. Here, $\dot{h}$ is velocity of the flapping motion, which is due to $-\delta u_P$ and $\delta u_T$ components, and $\dot{\theta}_{ref}$ is an angular velocity of the pitch motion with respect to the inertial frame. The perturbation term of $\dot{h}$ is represented above and $\dot{\theta}_{ref}$ is organized as follow.

$$\delta\theta_{ref} = -K_{p\beta}\beta - K_{p\varsigma}\varsigma + \alpha_y \cos\psi + \alpha_x \sin\psi \tag{16}$$

Figure 7 shows the damping of each wing mode, which are vertical bending ($q_1$), chordwise bending ($q_2$), and torsion ($p$) mode. They have similar trends with the wing modes based on the previous normal quasi-steady aerodynamic model. However the critical flight speed is slightly increased. It is clear that $q_1$ mode becomes unstable at approximately V = 550 ft/sec among the modes. The precise flutter boundary may be extracted by the system pole result obtained from the eigenvalue analysis.

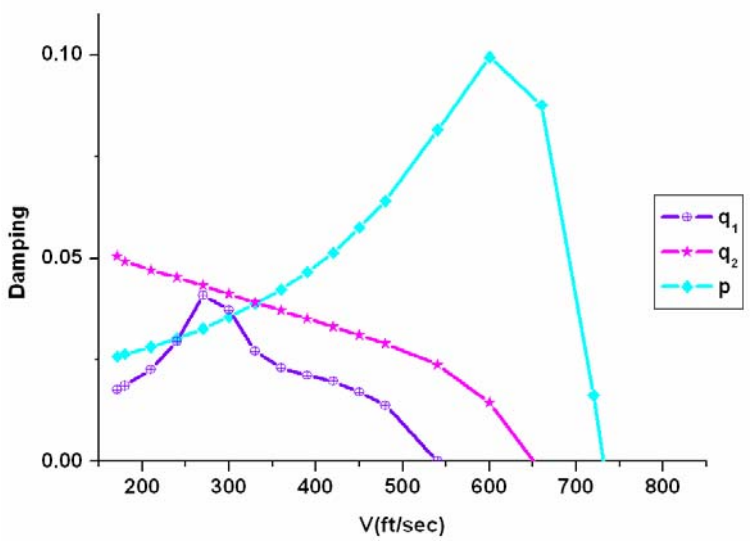


*Figure 7 : Damping of the modes in terms of the flight speed*

Figure 8 shows the eigenvalue results of whirl flutter stability using Greenberg's quasi-steady aerodynamics. According to the results, the flutter boundary is V=540 ft/sec. At this flight speed, the poles corresponding to the wing vertical bending mode ( $q_1$ ) are located on imaginary axis. There is a slight disagreement regarding the flutter boundary between the normal and Greenberg's aerodynamic model. Under the present Greenberg's quasi-steady aerodynamics, flutter occurs approximately 1% later than it does under the normal quasi-steady aerodynamics.

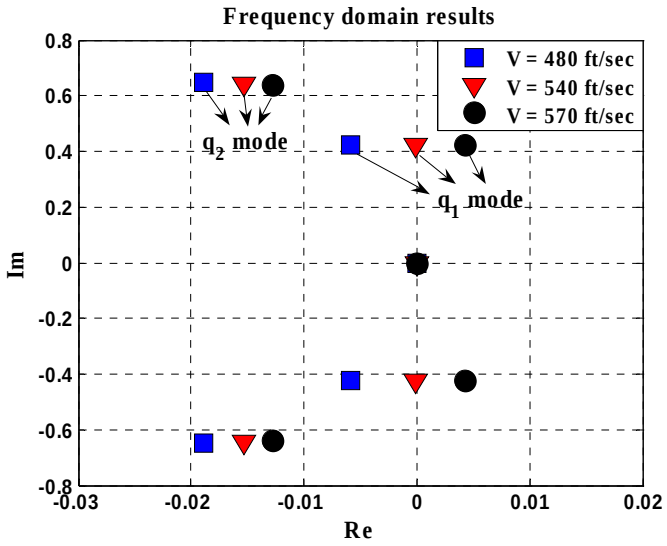


*Figure 8 : Frequency domain analysis using Greenberg's quasi-steady aerodynamics*

### 3.4 Full unsteady aerodynamic model

As mentioned previously, the quasi-steady aerodynamic model is not capable of describing a realistic aerodynamic environment occurring in tiltrotor aircraft. In this section, numerical investigation is conducted using Greenberg's two-dimensional unsteady aerodynamics.

Figure 9 illustrates the results of frequency domain analysis while increasing the flight speed from 540 to 660 ft/sec. The stability boundary is shown to be 642 ft/sec based on the full unsteady aerodynamics. The critical flight speed is predicted to be the highest under the full unsteady aerodynamics as compared with those based on the quasi-steady aerodynamic models. The whirl flutter stability is overestimated by the full unsteady aerodynamic model, by approximately 18% as compared with the result from the normal quasi-steady aerodynamic model.

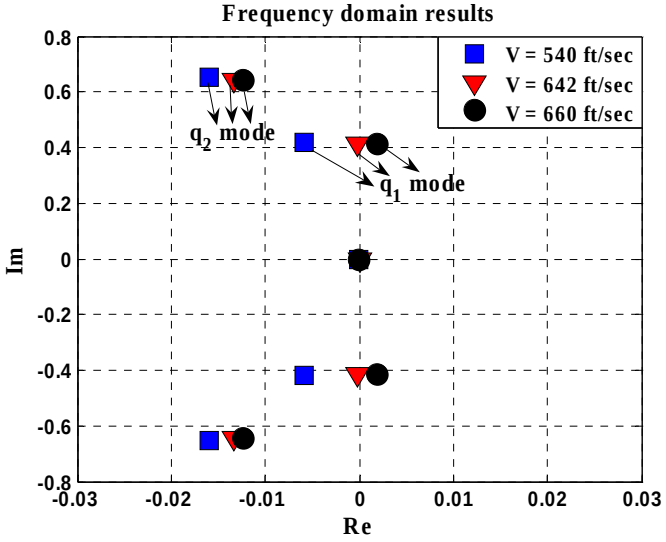


*Figure 9 : Frequency domain analysis using the full unsteady aerodynamics*

## 4. CONCLUSIONS

Time and frequency domain analyses are conducted with a newly developed analysis for whirl flutter stability in tiltrotor aircraft. The damping of each mode is also calculated. Two quasi-steady and an unsteady aerodynamic models are used to predict the whirl flutter stability boundary. Among them the flutter speeds based on the two quasi-steady aerodynamic models are approximately the same. However the full unsteady aerodynamics predicts the whirl flutter instability to occur at a higher speed than quasi-steady aerodynamic models do. Also, it is found that the modes concerned with flutter stability are the elastic wing modes.

In the future, a three-dimensional unsteady panel method is utilized to incorporate the wake effect for a rotor and wing aerodynamics, and then the aerodynamic interaction between rotor and wing will be considered with the wake model, because it induces a vibratory load on the flexible wing and fuselage. The wing is believed to be affected by the wake originated from the rotor. Elastic finite element modeled wing and blade torsion mode will also be utilized.

## ACKNOWLEDGMENTS

This study is supported by the KARI under KHP Dual-Use Component Development Program funded by the MOCIE. This work is also supported by grant No. R01-2005-000-10059-0 from the Basic Research Program of the Korea Science & Engineering Foundation, the Korea Research Foundation.

**REFERENCES**


[1] Hall, Jr., W. E., "Prop-Rotor Stability at High Advance Ratios," Journal of the American Helicopter Society, Vol. 11, (2), April 1966.

[2] Kvaternik, R. G., and Kohn, J. S., "An Experimental and Analytical Investigation of Proprotor Whirl Flutter," NASA technical paper-1047, Dec, 1977.

[3] Young, M. I., and Lytwyn, R. T., "The Influence of Blade Flapping Restraint on the Dynamic Stability of Low Disk Loading Propeller-Rotors," Journal of the American Helicopter Society, Vol. 12, (4), Oct. 1967, pp. 38-54.

[4] Johnson, W., "Dynamics of Tilting Proprotor Aircraft in Cruise Flight," NASA Technical Note D-7677, May, 1974.

[5] Johnson, W., "Analytical model for Tilting Proprotor Aircraft Dynamics Including Blade Torsion and Coupled Bending Modes, and Conversion Mode Operation," NASA TM X-62,369, August, 1974.

[6] Johnson, W., "Analytical Modeling Requirements for Tilting Proprotor Aircraft Dynamics," NASA TN D-8013, July, 1975.

[7] Nixon, M. W., Kvaternik, R. G., and Settle, T. B., "Tiltrotor Vibration Reduction Through Higher Harmonic Control," American Helicopter Society 53rd Annual Forum, Virginia Beach, Virginia, April 29-May 1, 1977.

[8] Kvaternik, R. G., Piatak, D. J., Nixon, M. W., Langston, C. W., Sigleton, J. D., Bennett, R. L., and Brown, R. K., "An Experimental Evaluation of Generalized Predictive Control for Tiltrotor Aeroelastic Stability Augmentation in Airplane Mode of Flight," American Helicopter Society 57th Annual Forum, Washington, DC, May 9-11, 2001.

[9] Singh, R. and Gandhi, F., "Wing Flaperon and Swashplate Control for Whirl Flutter Stability Augmentation of a Softinplane Tiltrotor," The 31st European Rotorcraft Forum, Florence, Italy, Sept. 13-15, 2005.

[10] Kim, T. and Shin, S. J., “Time and Frequency Domian Analysis of Whirl Flutter Stability in Tiltrotor Aircraft,” 47th AIAA/ASME/ASCE/AHS/ASC Structures, Structural Dynamics, and Materials Conference, Newport, RI, May 1-4, 2006.

[11] Kim, T. and Shin, S. J., “The Role of Unsteady Aerodynamic Interaction between Rotor and Wing in Tiltrotor Aircraft Whirl Flutter Instability,” International Forum on Aeroelasticity and Structural Dynamics 2007, Stockholm, Sweden, June 18-20, 2007.

[12] Hathaway, E. L., “Active and Passive Techniques for Tiltrotor Aeroelastic Stability Augmentation,” Ph.D. Thesis, The Graduate School College of Engineering, The Pennsylvania State University, August, 2005.

[13] Bisplinghoff, R. L., Ashley, H., and Halfman, R. L., Aeroelasticity, Dover, New York, 1996, Chaps. 6.

[14] Greenberg, J. M., “Airfoil in Sinusoidal Motion in Pulsating Stream,” NASA TN 1326, 1947.

[15] Cesnik, C. E. S., 16.242 Aeroelasticity, Lecture Note, Department of Aeronautics and Astronautics, Massachusetts Institute of Technology, Cambridge, Massachusetts, February 1998.

[16] Jones, R. T., “The Unsteady Lift of a Wing of Finite Aspect Ratio,” NACA Report 681, 1940.

[17] Jones, R. T., “Operational Treatment of the Nonuniform Lift Theory to Airplane Dynamics,” NACA TN 667, 1938.

[18] Friedmann, P. P. and Robinson, L. H., “Influence of Unsteady Aerodynamics on Rotor Blade Aeroelastic Stability and Response,” AIAA Journal, Vol. 28, No. 10, December 1990, pp. 1806-1812.

[19] Nixon, M. W., “Aeroelastic Response and Stability of Tiltrotors with Elastically-Coupled Composite Rotor Blades,” Ph.D. Thesis, University of Maryland, 1993.